Tuning electronic structure of monolayer InP3 in contact with graphene or Ni: Effect of a buffer layer and intrinsic In and P-vacancy

Journal:	*Physical Chemistry Chemical Physics*
Manuscript ID	CP-ART-10-2018-006478.R2
Article Type:	Paper
Date Submitted by the Author:	11-Dec-2018

Complete List of Authors:	Li, Zhongjun; Hefei University of Technology, School of Electronic Science and Applied Physics Qian, Mingzhi; Hefei University of Technology Song, Lingling; Hefei University of Technology Ma, Liang; University of Nebraska-Lincoln, Chemistry Qiu, Huaili; Hefei University of Technology, School of Electronic Science and Applied Physics Zeng, Xiao Cheng; University of Nebraska-Lincoln, Department of Chemistry

Tuning electronic structure of monolayer InP_3 in contact with graphene or Ni: Effect of a buffer layer and intrinsic In and P-vacancy

Zhongjun Li,[ab] Mingzhi Qian,[a] Lingling Song,[a] Liang Ma,[bd] Huaili Qiu[a] and Xiao Cheng Zeng[bc*]

[a] School of Electronic Science and Applied Physics, Hefei University of Technology, Hefei, Anhui 230009, China

[b] Department of Chemistry, University of Nebraska−Lincoln, Lincoln, Nebraska 68588, United States

[c] Department of Chemical & Biomolecular Engineering and Department of Mechanical and Materials Engineering, University of Nebraska−Lincoln, Lincoln, Nebraska 68588, United States

[d] School of Physics, Southeast University, Nanjing 211189, China

*E-mail: xzeng1@unl.edu

Abstract

Monolayer indium triphosphide (*m*-InP_3), predicted theoretically as a new 2D semiconducting material, exhibit promising opportunity for applications in electronic and optoelectronic devices. [J. Am. Chem. Soc. 2017, 139, 11125−11131]. For these applications, excellent contacting performance between *m*-InP_3 and electrodes is vital. In this work, by first principles calculations, electronic structures of *m*-InP_3 in contact with graphene (G) and Ni are investigated and the contacting characters are further tuned by inserting a buffer layer, e.g., G or BN monolayer (*m*-BN) along with introducing intrinsic P- and In-vacancy defects. For the *m*-InP_3 in contact with G, inserting an *m*-BN can alter the contacting character from an *n*-type to a *p*-type Schottky contact. This is consistent with the prediction of Schottky-Mott rule, indicating that Fermi level pinning is removed in the interface. However, for the contact with Ni, if an *m*-BN or G is inserted into the interface, an *n*-type Ohmic contact is obtained, rather than the *p*-type Schottky one based on Schottky-Mott rule. We attribute this inconsistency to the effect of electron transfer from *m*-BN or G to Ni, which leads to decreased work function of Ni. Additionally, introducing In- and P-vacancy defects can reduce Schottky barrier in the interfaces between *m*-InP_3 and G or Ni. Moreover, if *m*-BN is inserted into these defect-containing interfaces, an *n*-type Ohmic contact could be achieved and dominate the contacting character. Our results offer deeper insights into the factors such as the Fermi level pinning on the band alignment of the interfaces between *m*-InP_3 and G or Ni, and how the contacting characters are improved by inserting a buffer layer along with introducing In- and P-vacancy defects.

Keywords: monolayer indium triphosphide; Schottky barrier; Ohmic contact; work function match; Fermi level pinning

Introduction

With approaching the integration limit of silicon-based devices, two-dimensional (2D) atomically thin materials, such as graphene (G)[1-3], silicene[4-6], transition metal dichalcogenides[7-9], hexagonal arsenene[10-12], black phosphorus[13, 14] and VA/VIA topological insulators with few quintuple layers[15-17] have received considerable attention. The devices based on some of these 2D materials show small short channel effects, excellent electrostatic modulations, and high integration due to their ultrathin thickness[18, 19]. Hence, much effort has been made to explore 2D materials with suitable band gap, excellent electron mobility and high ambient stability[20, 21].

Recently, monolayer indium triphosphide (*m*-InP_3) was theoretically predicted by Miao et al.[22]. They showed that this 2D semiconducting material possesses high stability, a suitable band gap of 1.14 eV, and a high carrier mobility of 1919 $cm^2V^{-1}s^{-1}$. Moreover, through doping, *m*-InP_3 exhibits tunable magnetism and half-metallicity. Extraordinary optical absorption is also predicted over the entire visible light range[22]. As such, *m*-InP_3 appears to be a promising candidate for device applications. It is known that low contacting resistance in interface between 2D semiconductor and metal electrodes is a key requirement for high performance of the devices[23-25]. However, non-negligible contact resistance due to the Schottky barrier in interface can substantially lower carrier injection efficiency, and thus limit the performance of the devices[23-25]. Therefore, it is necessary to understand contacting properties between *m*-InP_3 and metallic materials for the potential device applications. To date, determination of the contacting performance between 2D semiconductors and metallic electrodes through exploration of the factors such as the Fermi level pinning is still an open topic[24-27].

According to the Schottky−Mott rule, it is generally accepted that metallic materials with low or high work functions can be utilized to obtain *n*-type or *p*-type Schottky contacts with 2D semiconductors, and the Ohmic contacts may be achieved by choosing metallic materials with suitable work function[23]. However, previous experimental and theoretical studies showed that Schottky barrier height in the interfaces between 2D semiconductors and metals generally deviates from the predictions of the Schottky-Mott rule, and the factors that cause the deviation are quite complex[23-26, 28, 29]. A match of the work function is insufficient to determine the contact characteristic[23-26, 28, 29]. One of the major factors is Fermi level pinning,

which would induce inflexible Schottky barrier, resulting in weak dependence of Schottky barrier height (SBH) on the work function, and thereby preventing the Ohmic contact formation in interfaces[23-26, 28]. While doping methods have been proposed to reduce SBH, limitations arise in the fabrication of devices, based on 2D semiconductors. For example, chloride doping in MoS_2 effectively lowers SBH but significantly shifts threshold voltage of the device. This shift is undesirable in the application of field effect transistor (FET)[30, 31]. Recent experimental studies also showed that inserting a buffer layer, such as hexagonal boron nitride (BN), into the interface can reduce contacting resistance between 2D semiconductors and metals[32-35]. But the number studies are scarce, and the mechanism responsible for the decreased contacting resistance still needs further investigation. If the deviation from the Schottky-Mott rule is removed, it would be straightforward to achieve the lowest contacting resistance by choosing suitable metals as electrodes, according to the work function match, for the devices based on 2D semiconductors[32-35].

In this work, our focus is placed on investigation of the contacting characters between *m*-InP_3 and metallic materials, and exploration of effective way to reduce contacting resistance. By using first principles calculations, we have computed electronic structures of the interfaces between *m*-InP_3 and G and nickel (Ni), as both are commonly employed as electrodes in nano devices[36-41]. Moreover, both G and Ni not only show slight lattice mismatch with *m*-InP_3 but also possess different work functions that can be compared regarding the influence of Fermi level pinning on the contacting characters of the interfaces. Consistent with previous studies, we found that G displays tunable Fermi level and low resistance, which can facilitate to tune contacting character in the experiments[36-38, 42]. To reduce the influence of Fermi level pinning, G and monolayer BN (*m*-BN) are used as the inserting layer for Ni and G electrode, respectively. The effects of interface bonding, electron transfer and electrostatic potential on the contacting character of the interfaces are also investigated.

2. Computational Method

The first-principles calculations are carried out based on density functional theory (DFT) within the projector augmented wave (PAW) method, implemented in the Vienna ab initio

simulation package (VASP 5.4)[43-45]. The generalized gradient approximation (GGA) of the Perdew, Burke and Ernzerhof (PBE) are employed to describe the exchange and correlation functional with the partial core correction included[46]. Structures of all six combined systems are presented in Fig. 1. A vacuum region of 20 Å normal to the 2D surface is added so that the interaction between adjacent slabs is negligible. To account for the van der Waals (vdW) interaction, the DFT-D3 method with Becke-Jonson damping is used in all calculations[47]. The (111) surfaces of Ni is chosen as it is shown to be the most stable in the previous experiments[48, 49]. To simulate the surfaces, the Ni slab is extended to the fourth atomic layer. It is known that the GGA-PBE functional generally underestimates the band gaps of semiconductors. Several more accurate theoretical methods, such as HSE06 functional and GW method, can be used to accurately predict electronic structures for small systems[50, 51]. For large systems considered in this study, however, the GGA-PBE functional is only practical with our computing resources, and yet it can still predict reliable trend of electronic structures.

For DFT computations, geometric structures are relaxed until the force on each atom is less than 0.01 eV/Å. The convergence criteria are 10^{-4} eV for energy. During the ionic relaxation, the shape and size of the supercell are fixed, while all atoms are fully relaxed except that the Ni atoms in the two bottom atomic layers are fixed at their bulk positions. The Monkhorst-Pack k-point sampling in Brillouin zone is Γ-centered with 9×9×1 and 15×15×1 meshes in ionic and electronic optimization, respectively. A cutoff energy of 450 eV is chosen for the plane-wave basis set.

To evaluate the stability of all combined systems, the binding energy between *m*-InP_3 and G, *m*-BN or Ni is calculated by the following formula

$$E_f = E_t - (E_1 + E_2) \quad (1)$$

where E_1, E_2 and E_t denote the energy of isolated system 1, isolated system 2, and the corresponding combined system, respectively. The electron density difference between the two-isolated systems and the combined system is performed according to the following formula

$$\Delta\rho = \rho_t - (\rho_1 + \rho_2) \quad (2)$$

where the electron densities of ρ_1, ρ_2 and ρ_t are averaged over the planes parallel to the

interface. Through the electron density difference analysis, the electron transfer and redistribution along the Z-direction normal to the interface is obtained.

The SBH between *m*-InP_3 and metallic G or Ni is calculated according to the Schottky−Mott rule to evaluate the contacting characters of the interfaces. The SBH for electrons (Φ_e) is defined as

$$\Phi_e = E_{CBM} - E_F \quad (3)$$

and that for holes (Φ_h) is defined as

$$\Phi_h = E_F - E_{VBM} \quad (4)$$

where E_F is the Fermi level, and E_{CBM} and E_{VBM} are the conduction band minimum and the valence band maximum of the semiconductor, respectively.

Table 1 Equilibrium interface distance (d/Å) and formation energy per unit cell (E_f/eV) for the six systems, by combining *m*-InP_3 with G, *m*-BN or Ni.

	m-InP_3@G	*m*-InP_3@*m*-BN	*m*-InP_3@Ni	*m*-InP_3@*m*-BN@G	*m*-InP_3@*m*-BN@Ni	*m*-InP_3@G@Ni
d_1	3.31	3.25	1.77	3.18	3.06	3.12
d_2				3.54	2.08	2.07
E_{f1}	-0.70	-0.76	-7.98	-0.84	-1.18	-1.11
E_{f2}				-0.83	-3.38	-2.39

3. Results and discussion

The stacking configurations of *m*-InP_3 in direct contact with G, *m*-BN or Ni are shown in Fig. 1, as well as those with a buffer layer of G or *m*-BN in between. We denote these configurations as *m*-InP_3@G, *m*-InP_3@*m*-BN, *m*-InP_3@Ni, *m*-InP_3@*m*-BN@G, *m*-InP_3@G@Ni and *m*-InP_3@*m*-BN@Ni, respectively. The separations of interface are denoted by d_1 and d_2. For *m*-InP_3, the optimized lattice constant is 7.56 Å, consistent with previous theoretical result[22]. For all six systems, the lattice constant of *m*-InP_3 is constantly kept to be 7.56 Å, while the 3×3×1 supercells of *m*-BN, G, and (111) surface slab of Ni are slightly extended to match the 1×1×1 primitive cell of *m*-InP_3. As a result, the mismatch is

less than 1%. To investigate effects of defects on the contacting character, intrinsic P- and In-vacancy are introduced in 2×2×1 supercell of *m*-InP_3.

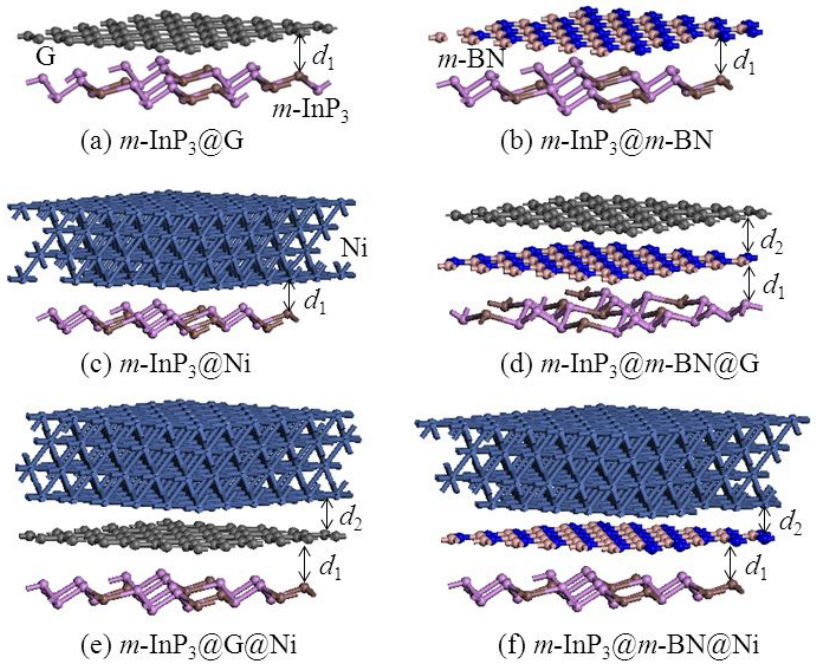

Fig. 1 Schematics of the *m*-InP_3 combined with (a) G, (b) *m*-BN, (c) Ni, (d) *m*-BN and G, (e) G and Ni, and (f) *m*-BN and Ni. The separations of interface are denoted by d_1 and d_2.

3.1. *m*-InP_3@G, *m*-InP_3@*m*-BN and *m*-InP_3@Ni

As listed in Table 1, for the *m*-InP_3@G, *m*-InP_3@*m*-BN and *m*-InP_3@Ni systems, the optimized interfacial distances are 3.31 Å, 3.25 Å, and 1.77 Å, with the corresponding formation energies being –0.70 , –0.76 and –7.98 eV, respectively. These results suggest weak interaction between *m*-InP_3 and G or *m*-BN, but strong bonding interaction between *m*-InP_3 and Ni. Also, the interfacial interaction in the *m*-InP_3@G system is slightly weaker than that in *m*-InP_3@*m*-BN.

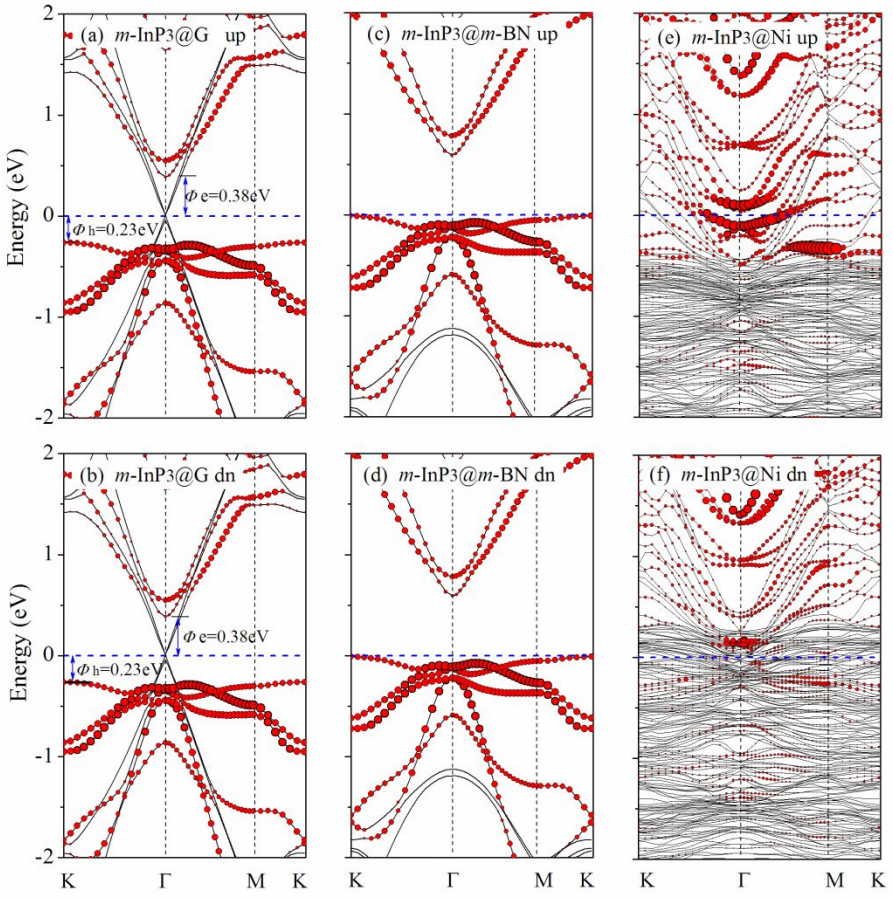

Fig. 2 Spin-polarized band structures of m-InP_3@G, m-InP_3@m-BN and m-InP_3@Ni. Blue dash lines indicate Fermi level, and red dots represent the band structures projected on m-InP_3, while the dot size denotes the weight.

Computed spin-polarized band structures of m-InP_3@G, m-InP_3@m-BN and m-InP_3@Ni are shown in Fig. 2. The red dots represent the band structures projected on m-InP_3. From Fig. 2(a)–(d) one can see that in the m-InP_3@G and m-InP_3@m-BN systems, m-InP_3 and m-BN retain semiconducting character, and G keeps semimetallic character with the Fermi level through the Dirac point. In m-InP_3@G, according to the Eqs. (3) and (4), the SBH of 0.38 and 0.23 eV for electrons and holes are obtained from the band alignments, respectively, as shown in Fig. 2(a) and (b). In the m-InP_3@Ni system, the band structure projected on Ni is spin-polarized. Due to strong interaction with Ni, m-InP_3 is metalized and its band structure shows partial spin-polarized character (see Fig. 2(e)–(f)). Due to different coupling intensity, the interface between m-InP_3 and G is p-type Schottky contact, whereas the contact between

m-InP_3 and Ni is generally Ohmic. The difference in the coupling intensity is consistent with the different interfacial distances and formation energies for the three interfaces discussed above. Fig. 2(e) and 2(f) show that near the Fermi level, the electronic states of spin-up channel are mainly contributed from *m*-InP_3, while those of spin-down channel are dominated by Ni. Thus, although the direct contact between *m*-InP_3 and Ni leads to the metallization of *m*-InP_3, the conducting character of the interface is still weak.

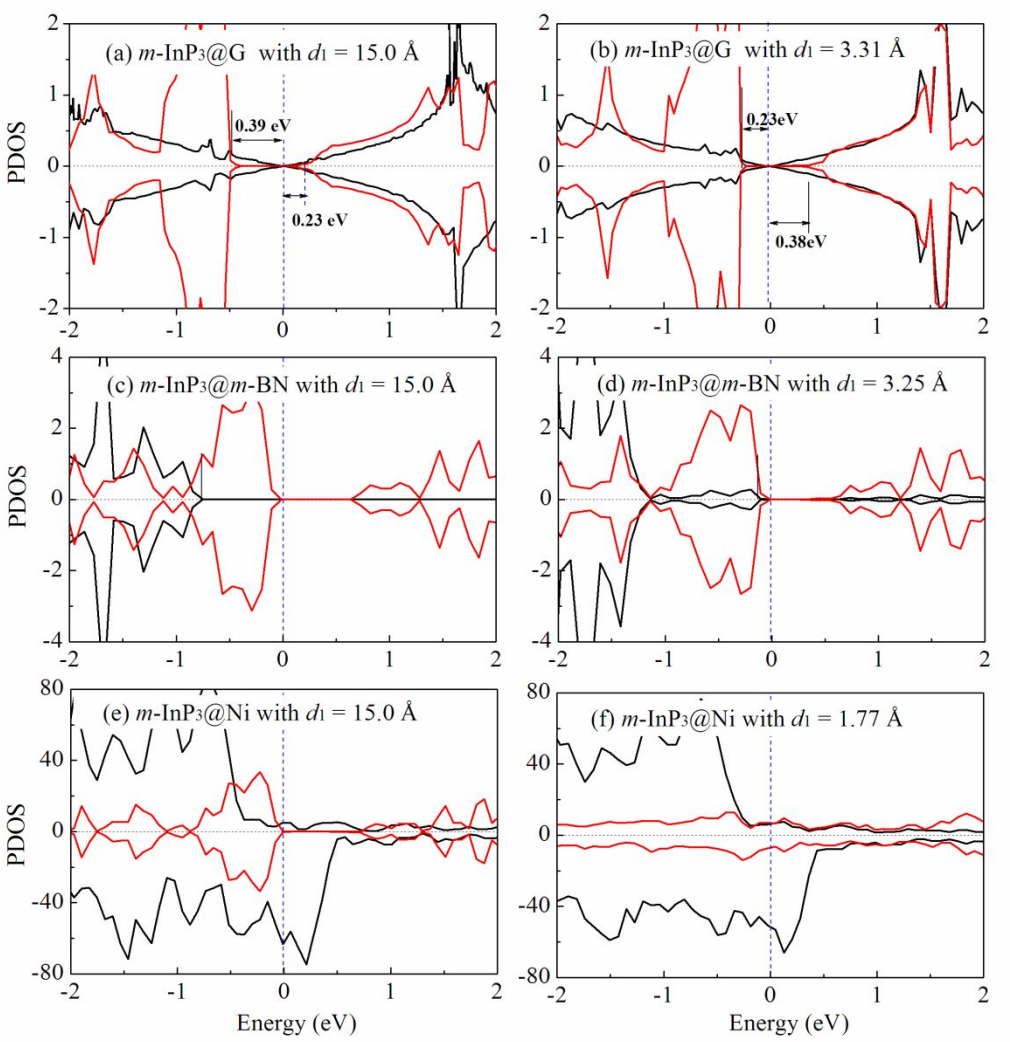

Fig. 3 Computed spin-polarized PDOS, for *m*-InP_3 being in contact with G, *m*-BN or Ni with interfacial distance of 15 Å and with optimized interfacial distance, respectively. In panels (a) and (b) the marked SBH are extracted from the band structure alignments of Fig. 2(a), 2(b) and Fig. S1 (ESI) by Eqs. (3) and (4).

In order to comparatively investigate the effects of contacts on electronic structures, especially on band alignment and the Fermi level pinning, the spin-polarized partial density of

states (PDOS) of *m*-InP_3@G, *m*-InP_3@*m*-BN and *m*-InP_3@Ni at the optimized interfacial distances are presented in Fig. 3, together with those at the interfacial distance of 15 Å. This distance is long enough to neglect the interfacial interaction. To show the quantitative changes of contacting characters with the interface distances, in the PDOS of Fig. 3(a) and 3(b), we marked the SBH extracted from Fig. 2(a), 2(b) and Fig. S1 (ESI) by Eqs. (3) and (4). It can be seen from Fig. 3(a) and S1 (ESI) that when the interfacial distance is about 15 Å, the band alignment between *m*-InP_3 and G exhibits an *n*-type Schottky contact, with a barrier height about 0.23 eV. The interfacial interaction can be neglected, and according to the Schottky-Mott rule the contacting character is determined by the work-function match. Nevertheless, with *m*-InP_3 contacting with G, the interface becomes *p*-type Schottky contact with a barrier about 0.23 eV (Fig. 3(b)). It is worth noting that when *m*-InP_3 is in direct contact with G, the Fermi level shifts toward the valence band of *m*-InP_3. This character differs from the case of semiconductors in direct contact with typical metals, where the Fermi level is generally pinned near the conducting band of semiconductors.[25, 28]

In the *m*-InP_3@*m*-BN system, the band gap of both monolayers also decreases, as shown in Fig. 3(c)–(d). The optimized interfacial distances listed in Table 1 show that the interfacial coupling in the *m*-InP_3@G or *m*-InP_3@*m*-BN is vdW interaction in nature. From the PDOS, one can see that the effects of the interfacial interaction on the electronic structures are important. The band gap of the *m*-InP_3, when in contact with *m*-BN, decreases notably than that in the contact with G, due to stronger interaction in the former. According to the work-function match, when *m*-InP_3 is in contact with Ni, considering spin-polarized character of Ni, the spin-up and spin-down channels should be p-type Ohmic and weak p-type Schottky, respectively. When *m*-InP_3 is in direct contact with Ni, *m*-InP_3 is metalized, and the *n*-type Ohmic contact arises for both spin channels (see Fig. 3(e) and (f)).

To understand the contacting characters from the perspective of electron transfer and electrostatic potential distribution, the plane averaged electron density difference along Z-direction (normal to interface) is plotted in Fig. S2 (ESI), together with the plane averaged electrostatic potential for *m*-InP_3@G, *m*-InP_3@*m*-BN and *m*-InP_3@Ni, respectively. As shown in Fig. S2(a) and (b) (ESI), when *m*-InP_3 is in contact with G or *m*-BN, minor electron transfer occurs from two sides of G or *m*-BN to the interfacial region near *m*-InP_3. As a result, a weak

dipole layer forms in the interface. In the G and *m*-BN layers minor electron accumulation appears. When Ni is in contact with *m*-InP_3, major electron transfer from Ni to *m*-InP_3 results in the substantial interface bonding, while a strong dipole layer forms in the interface, as shown in Fig. S2(c) (ESI). The 3D charge density difference (Fig. S4 of ESI) gives more detailed electron transfer redistribution as the interface forms. The plane averaged electrostatic potential in Fig. S2(d)−(f) (ESI) indicates that the Fermi levels of the three systems are higher than the maximum of electrostatic potentials in the interfaces, suggesting no electrostatic-potential barrier for electron tunneling through the interface.

From above description one can see that when *m*-InP_3 is in contact with G, *m*-BN and Ni, the contacting characters at the interface are determined not merely by work-function match. Electron transfer and the associated dipole layer and interlayer bonding at the interface also play important roles on the contacting characters. In particular, according to the work function match, it is expected that the *m*-InP_3 in contact with G should be n-type Schottky interface. However, the strong interfacial dipole results in a p-type Schottky contact. This unexpected result leads to complexity and uncertainty in selecting and design of electrode materials. In order to make the contacting characters more sensitive to work function, either *m*-BN or G is examined as an inserting layer to greatly weaken the influence of interfacial interaction.

3.2. Effects of inserting a buffer layer: *m*-InP_3@*m*-BN@G, *m*-InP_3@*m*-BN@Ni and *m*-InP_3@G@Ni

Spin-polarized band structures and PDOS of *m*-InP_3@*m*-BN@G, *m*-InP_3@G@Ni and *m*-InP_3@*m*-BN@Ni are presented in Fig. 4. Clearly, in the *m*-InP_3@*m*-BN@G system, *m*-InP_3 and *m*-BN retains semiconducting character and G keeps semi-metallic quantity. The interface between *m*-InP_3 and G is n-type Schottky contact with a barrier about 0.21 eV. This conducting character is quantitatively consistent with that predicted from the work function match (Fig. 3(a) and Fig. S1 of ESI), indicating that *m*-BN, a vdW inserting layer, can effectively remove the interfacial coupling between *m*-InP_3 and G.

As discussed in Section 3.1, chemical bonding leads to the metallization of *m*-InP_3 in the system of *m*-InP_3@Ni. In general, despite of metallization, the Schottky barrier would transfer to the interface between the metalized complex of *m*-InP_3@Ni and the *m*-InP_3 in the channel

of device[26, 29]. To remove interfacial bonding and avoid the transfer of Schottky barrier, buffer layer like G or *m*-BN can be inserted into the interface between *m*-InP_3 and Ni. Different from the direct contact with Ni, in both *m*-InP_3@*m*-BN@Ni and *m*-InP_3@G@Ni systems, *m*-InP_3 retains semiconducting character, as shown in Fig. 4(b) and (c). Due to the interaction induced by the direct contact with Ni, both *m*-BN and G are now metallized in various degrees. Therefore, in these two systems, the contacting characters of the interfaces are determined not only by the work function, but also by interfacial coupling between Ni and the inserting layer, differing from the case of *m*-InP_3@*m*-BN@G. As such, n-type Ohmic contacts are achieved in spin-up and spin-down channels, as shown in Fig. 4(b) and (c). However, near the Fermi level in spin-up channel, the PDOS contributed from Ni is little. Therefore, the contacting characters of the *m*-InP_3@*m*-BN@Ni and *m*-InP_3@G@Ni systems are dominated by n-type Ohmic contacts in spin-down channel.

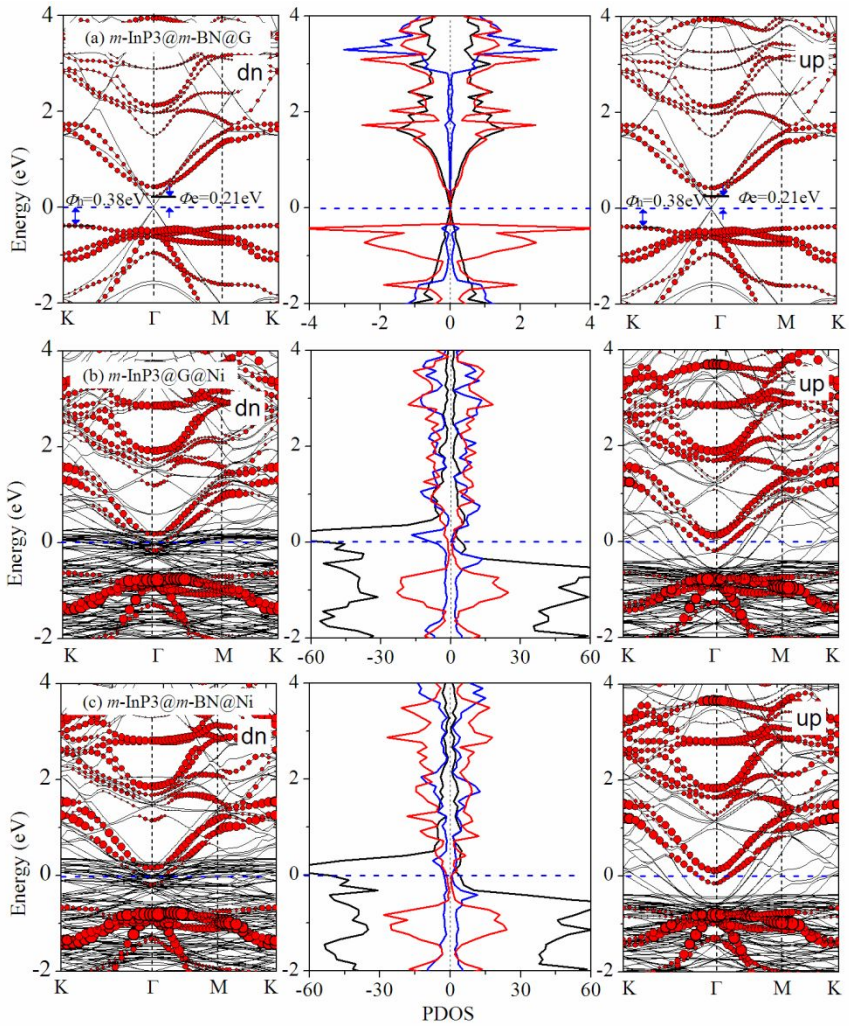

Fig. 4 Spin-polarized band structures and PDOS for (a) *m*-InP_3@*m*-BN@G, (b) *m*-InP_3@G@Ni and (c) *m*-InP_3@*m*-BN@Ni. In the band structures, red dots represent the band projected on *m*-InP_3 and the dot size denotes the weight. In PDOS, the black, blue and red lines denote the contribution from G or Ni, the inserted layer *m*-BN or G, and *m*-InP_3, respectively.

The effects of inserting a buffer layer on the contacting characters of the *m*-InP_3@*m*-BN@G, *m*-InP_3@*m*-BN@Ni, and *m*-InP_3@G@Ni systems can be understood by analyzing their plane averaged electron density difference and plane averaged electrostatic potential. For the *m*-InP_3@*m*-BN@G system, a dipole layer forms in the interface between *m*-InP_3 and *m*-BN, as in the case of *m*-InP_3@G or *m*-InP_3@*m*-BN system. An obvious difference from the *m*-InP_3@*m*-BN@G system is that minor electron accumulation appears near G in the *m*-InP_3@*m*-BN@G system, as shown in Figs. S3(a) and S4(d). Thus, the G layer in *m*-InP_3@*m*-BN@G almost keeps the same electronic structure, and the band alignment in the interface can be determined by the work-function match between *m*-InP_3 and G. For the *m*-InP_3@*m*-BN@Ni system, two regions of electron accumulation arise in the interface between *m*-InP_3 and *m*-BN. Between the two regions, an electron-depletion region appears. Consequently, two dipole layers with opposite dipole direction are formed and their influences are substantially offset by one another[32-35]. In the interface between *m*-BN and Ni, there is a notable electron-depletion region next to *m*-BN, and two notable accumulation regions are close to the Ni layer. This major electron transfer to Ni layer leads to notable decrease of the work function of the Ni layer. The electron transfer character in the *m*-InP_3@G@Ni system is similar to that in the *m*-InP_3@m-BN@Ni system, as shown in Fig. S3 and S4 (ESI).

From the above discussion one can conclude that in *m*-InP_3@*m*-BN@G, inserting an *m*-BN layer can keep electronic structures of G and *m*-InP_3 as their pristine ones, and electron transfer between G and *m*-BN can be negligible. Therefore, the Fermi level pinning between *m*-InP_3 and G is removed, and the band alignment between them is only determined by their work-function match. In the *m*-InP_3@*m*-BN@Ni and *m*-InP_3@G@Ni systems, the introduction of *m*-BN or G layer makes electronic structures of *m*-InP_3 as the pristine one, but the electron transfer from *m*-BN or G to Ni clearly reduces the work function of Ni. Thus, the

band alignment between *m*-InP_3 and Ni depends weakly on their work-function match. Despite of this weak dependence, we find that the contacting performance of the interface between *m*-InP_3 and Ni is markedly improved by inserting a buffer layer of *m*-BN or G.

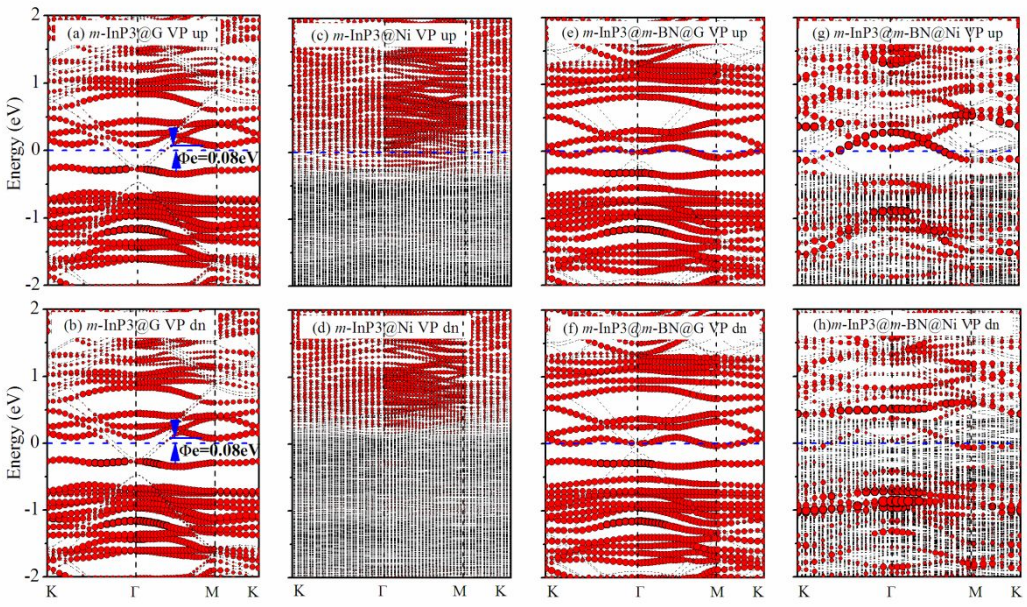

Fig. 5 Spin-polarized band structures of *m*-InP_3@G, *m*-InP_3@Ni, *m*-InP_3@*m*-BN@G and *m*-InP_3@*m*-BN@Ni with P-vacancy defect (VP). The red dots represent the projected band on *m*-InP_3 and the dot size denotes the weight.

3.3. Effects of P- and In-vacancy defects for *m*-InP_3@G, *m*-InP_3@Ni, *m*-InP_3@*m*-BN@G and *m*-InP_3@*m*-BN@Ni

As is known, intrinsic vacancy defects are ubiquitous during the material preparation and device assembly[27, 52]. Formation energies of 1×1, 2×2 and 3×3 supercells of *m*-InP_3 with P-vacancy and In-vacancy defects (denoted as VP and VIn, respectively) are listed in Table S1, and the evolution of the band structures is presented in Fig. S5 (ESI). Here, effects of P- and In-vacancy defects on the electronic structures and contacting characters of the interfaces in the four systems, *m*-InP_3@G, *m*-InP_3@Ni, *m*-InP_3@*m*-BN@G and *m*-InP_3@*m*-BN@Ni, are investigated. Considering the changes of electronic structures with different supercell sizes, only the 2×2 supercell of *m*-InP_3 with VP and VIn is employed in the four systems. Their spin-polarized band structures and PDOS are presented in Figs. 5 and S6, respectively.

Fig. 5(a), (b), (e) and (f) show that the interface of the *m*-InP_3@G system with VP is n-type

Schottky contact with a barrier of ~0.08 eV. When *m*-BN is inserted into the interface, the contact turns into an n-type Ohmic one. Thus, compared to the system without the defect, introducing P-vacancy is favorable to electron injection from G to *m*-InP_3 in *m*-InP_3@G and *m*-InP_3@*m*-BN@G.

Fig. 5(c) and (g) indicate that in *m*-InP_3@Ni and *m*-InP_3@*m*-BN@Ni with VP, although the spin-up channels are Ohmic, electron injection efficiency should be low due to the weak electronic states of Ni near the Fermi level, which can be clearly seen from PDOS in Fig. S6(d) (ESI). Fig. 5(d) and (h) show that spin-down channels of *m*-InP_3@Ni and *m*-InP_3@*m*-BN@Ni with VP are also Ohmic. However, it is noted that the contribution from spin-down state of *m*-InP_3 in the former system is weak near the Fermi level, and thus the carrier injection efficiency is low. Considering the essential contribution of *m*-InP_3 and Ni to spin-down state near the Fermi level in the *m*-InP_3@*m*-BN@Ni system with VP, we can draw a conclusion that introduction of the P-vacancy defect and inserting *m*-BN sheet can facilitate electron injection from Ni to *m*-InP_3 in the spin-down channel.

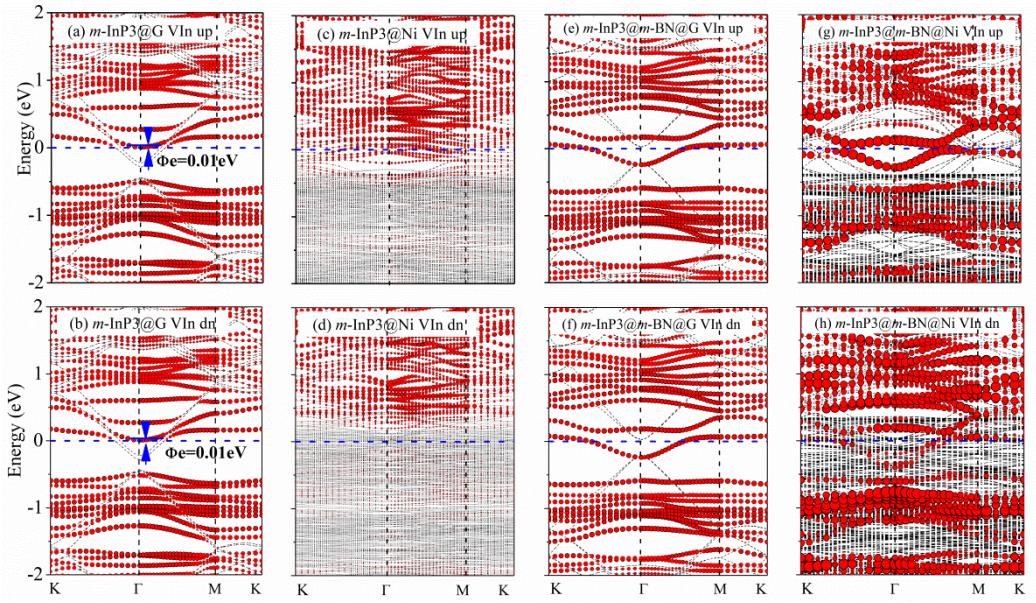

Fig. 6 Spin-polarized band structures of *m*-InP_3@G, *m*-InP_3@Ni, *m*-InP_3@*m*-BN@G and *m*-InP_3@*m*-BN@Ni with In-vacancy defect (VIn). The red dots represent the projected band on *m*-InP_3 and the dot size denotes the weight.

Here we discuss the difference in the band structures contributed from *m*-InP_3 in both

m-InP_3@*m*-BN@G and *m*-InP_3@*m*-BN@Ni systems with VP. In both systems, the band alignments are similar to each other. However, in *m*-InP_3@*m*-BN@Ni, although there is an inserting buffer layer of *m*-BN, the projected band structures on *m*-InP_3 differ from those in *m*-InP_3@*m*-BN@G. This difference can be attributed to the indirect effect of Ni. As disclosed by PDOS in Fig. S6 (ESI), in *m*-InP_3@*m*-BN@Ni with VP, due to the interaction with Ni, the electronic structure of *m*-BN is clearly changed. This further induces changes of electronic structures of *m*-InP_3 in *m*-InP_3@*m*-BN@Ni. Thus the *m*-InP_3 with VP in *m*-InP_3@*m*-BN@Ni exhibits different band structures from that in *m*-InP_3@*m*-BN@G.

Fig. 6 and S7 present the spin-polarized band structures and the corresponding PDOS of *m*-InP_3@G, *m*-InP_3@Ni, *m*-InP_3@*m*-BN@G and *m*-InP_3@*m*-BN@Ni with In-vacancy defects, respectively. The contacting character in the interface of *m*-InP_3@G is an n-type Schottky contact with a barrier about 0.01 eV. It transfers to an Ohmic contact with a buffer layer of *m*-BN, as shown in Fig. 6(a), (b), (e) and (f). When *m*-InP_3 is in direct contact with Ni, *m*-InP_3 is metallized in various degrees in spin-up and spin-down states. Near the Fermi level, for spin-up states, the contribution from Ni is very weak while for spin-down state the contribution from *m*-InP_3 is weak, as shown in Fig. 6(c), (d) and S7(b). Therefore, the interface of *m*-InP_3@Ni with In-vacancy defect should exhibit weak conducting character, similar to the case of *m*-InP_3@Ni with P-vacancy defect. When *m*-BN is inserted into the interface of *m*-InP_3@Ni with In-vacancy defect, the effect of Ni on the electronic structure of *m*-InP_3 can be neglected, as shown in Fig. 6(g) and (h). Because the contribution from spin-up states of Ni near the Fermi level is weak, electron injection through the interface is dominated by spin-down channel in *m*-InP_3@*m*-BN@Ni with In-vacancy defect. In addition, the contacting performance of the interfaces in the *m*-InP_3@G, *m*-InP_3@Ni, *m*-InP_3@*m*-BN@G and *m*-InP_3@*m*-BN@Ni systems with VP and VIn can be further evaluated by analyzing electron density difference and electrostatic potential distribution, as shown in Figs. S8 and S9.

4. Conclusions

In this work, we have studied electronic structures of *m*-InP_3 in direct contact with G, *m*-BN or Ni by using first principles calculations. Our focus is placed on tuning the contacting

characters (including band alignment) by inserting buffer layers and by introducing intrinsic vacancy defects in the interfaces. Consistent with many previous studies, we find that the contacting characters of the *m*-InP_3 in direct contact with G or Ni cannot be described by the Schottky-Mott rule. In direct contact with G, a p-type Schottky contact occurs, but not an n-type contact as predicted by the Schottky-Mott rule. In direct contact with Ni, the contacting character is n-type Ohmic due to the metallization of *m*-InP_3 through the interfacial bonding. Nevertheless, the low overlap of electronic states of Ni and *m*-InP_3 near the Fermi level in spin-up and spin-down channels may lead to low electron-injection efficiency from Ni to *m*-InP_3.

To remove the Fermi level pinning and interfacial bonding, either *m*-BN or G is employed as the inserting buffer layer. When *m*-BN is inserted into the interface between *m*-InP_3 and G, a transition from p-type to n-type Schottky contact occurs and the barrier height is consistent with the prediction of the Schottky-Mott rule, i.e., the Fermi level pining is removed. However, with inserting *m*-BN or G into the interface between *m*-InP_3 and Ni, an n-type Ohmic contact arises in spin-down channel, rather than the p-type Schottky contact as predicted by Schottky-Mott rule. This inconsistency can be attributed to the fact that obvious electron transfer from the inserting layer of *m*-BN or G to Ni leads to a decrease of work function of Ni. Thus, the band alignment between *m*-InP_3 and Ni cannot be described by the work-function match.

To further tune the contacting character of the interface between *m*-InP_3 and G or Ni, the In- and P-vacancy defects along with the buffer layer are introduced to the interface. It is found that the vacancy defects can induce gap states and obviously lower SBH. Inserting the buffer layer can weaken the interfacial interaction. Combining both approaches can tune the band alignment, and the transition from n-type Schottky to Ohmic contacts can be achieved for *m*-InP_3@G and *m*-InP_3@Ni with In- and P-vacancy defects. Thus, the contacting characters of the interfaces can be improved substantially.

Our results provide deeper insights into the factors such as Fermi level pinning to determine the band alignment of the interfaces between *m*-InP_3 and G or Ni, and the contacting characters can be improved appreciably by inserting a buffer layer and by introducing vacancy defects. Knowledge obtained from this study may be used as a guide for

selecting more effective electrode materials based on 2D *m*-InP_3.

Conflicts of interest

There are no conflicts to declare.

Acknowledgements

This work was partially supported by Anhui Natural Science Foundation of China (No. 1708085ME122), National Natural Science Foundation of China (NSFC) (No. 21503061) and Fundamental Research Funds for the Central Universities (JZ2015HGXJ0184, JZ2016HGBZ1046). X.C.Z. was supported by U.S. National Science Foundation through the Nebraska Materials Research Science and Engineering Center (MRSEC) (Grant No. DMR-1420645) and UNL Holland Computing Center.

References

1. A. K. Geim and K. S. Novoselov, *Nat. Mater.*, 2007, **6**, 183-191.
2. J. C. Meyer, A. K. Geim, M. I. Katsnelson, K. S. Novoselov, T. J. Booth and S. Roth, *Nature*, 2007, **446**, 60-63.
3. D. Halbertal, M. Ben Shalom, A. Uri, K. Bagani, A. Y. Meltzer, I. Marcus, Y. Myasoedov, J. Birkbeck, L. S. Levitov, A. K. Geim and E. Zeldov, *Science*, 2017, **358**, 1303-1306.
4. C. C. Liu, W. X. Feng and Y. G. Yao, *Phys. Rev. Lett.*, 2011, **107**, 076802.
5. J. J. Zhao, H. S. Liu, Z. M. Yu, R. G. Quhe, S. Zhou, Y. Y. Wang, C. C. Liu, H. X. Zhong, N. N. Han, J. Lu, Y. G. Yao and K. H. Wu, *Prog. Mater. Sci.*, 2016, **83**, 24-151.
6. B. Aufray, A. Kara, S. Vizzini, H. Oughaddou, C. Leandri, B. Ealet and G. Le Lay, *Appl. Phys. Lett.*, 2010, **96**, 183102.
7. S. Manzeli, D. Ovchinnikov, D. Pasquier, O. V. Yazyev and A. Kis, *Nat. Rev. Mater.*, 2017, **2**, 17033.
8. A. Kumar and P. K. Ahluwalia, *Eur. Phys. J. B*, 2012, **85**, 186.
9. Q. H. Wang, K. Kalantar-Zadeh, A. Kis, J. N. Coleman and M. S. Strano, *Nat. Nanotechnol.*, 2012, **7**, 699-712.
10. S. L. Zhang, Z. Yan, Y. F. Li, Z. F. Chen and H. B. Zeng, *Angew. Chem.-Int. Edit.*, 2015, **54**, 3112-3115.
11. Z. J. Li, W. Xu, Y. Q. Yu, H. Y. Du, K. Zhen, J. Wang, L. B. Luo, H. L. Qiu and X. B. Yang, *J Mater. Chem. C*, 2016, **4**, 362-370.
12. S. L. Zhang, S. Y. Guo, Z. F. Chen, Y. L. Wang, H. J. Gao, J. Gomez-Herrero, P. Ares, F. Zamora, Z. Zhu and H. B. Zeng, *Chem. Soc. Rev.*, 2018, **47**, 982-1021.
13. H. Liu, Y. C. Du, Y. X. Deng and P. D. Ye, *Chem. Soc. Rev.*, 2015, **44**, 2732-2743.
14. R. X. Fei and L. Yang, *Nano Lett.*, 2014, **14**, 2884-2889.
15. H. J. Zhang, C. X. Liu, X. L. Qi, X. Dai, Z. Fang and S. C. Zhang, *Nat. Phys.*, 2009, **5**, 438-442.

16. Y. Liu, Y. Y. Li, S. Rajput, D. Gilks, L. Lari, P. L. Galindo, M. Weinert, V. K. Lazarov and L. Li, *Nat. Phys.*, 2014, **10**, 294-299.
17. Z. J. Li, S. Chen, J. Y. Sun, X. X. Li, H. L. Qiu and J. L. Yang, *J Phys-Condens Mat.*, 2018, **30**, 065503.
18. H. Liu, A. T. Neal and P. D. D. Ye, *Acs Nano*, 2012, **6**, 8563-8569.
19. S. Ghatak and A. Ghosh, *Appl. Phys. Lett.*, 2013, **103**, 122103.
20. X. X. Li, X. J. Wu and J. L. Yang, *J Am. Chem. Soc.*, 2014, **136**, 5664-5669.
21. T. Hu, H. P. Wu, H. B. Zeng, K. M. Deng and E. Kan, *Nano Lett.*, 2016, **16**, 8015-8020.
22. N. H. Miao, B. Xu, N. C. Bristowe, J. Zhou and Z. M. Sun, *J Am. Chem. Soc.*, 2017, **139**, 11125-11131.
23. Y. Liu, J. Guo, E. B. Zhu, L. Liao, S. J. Lee, M. N. Ding, I. Shakir, V. Gambin, Y. Huang and X. F. Duan, *Nature*, 2018, **557**, 696-700.
24. C. Kim, I. Moon, D. Lee, M. S. Choi, F. Ahmed, S. Nam, Y. Cho, H. J. Shin, S. Park and W. J. Yoo, *Acs Nano*, 2017, **11**, 1588-1596.
25. S. Das, H. Y. Chen, A. V. Penumatcha and J. Appenzeller, *Nano Lett.*, 2013, **13**, 100-105.
26. Z. J. Li, X. X. Li and J. L. Yang, *ACS Appl. Mater. & Inter.*, 2015, **7**, 12981-12987.
27. J. H. Park, A. Sanne, Y. Z. Guo, M. Amani, K. H. Zhang, H. C. P. Movva, J. A. Robinson, A. Javey, J. Robertson, S. K. Banerjee and A. C. Kummel, *Sci. Adv.*, 2017, **3**, 1701661.
28. C. Gong, L. Colombo, R. M. Wallace and K. Cho, *Nano Lett.*, 2014, **14**, 1714-1720.
29. J. H. Kang, W. Liu, D. Sarkar, D. Jena and K. Banerjee, *Phys. Rev. X*, 2014, **4**, 031005.
30. L. M. Yang, K. Majumdar, H. Liu, Y. C. Du, H. Wu, M. Hatzistergos, P. Y. Hung, R. Tieckelmann, W. Tsai, C. Hobbs and P. D. Ye, *Nano Lett.*, 2014, **14**, 6275-6280.
31. X. F. Li, L. M. Yang, M. W. Si, S. C. Li, M. Q. Huang, P. D. Ye and Y. Q. Wu, *Adv. Mater.*, 2015, **27**, 1547-1552.
32. J. L. Wang, Q. Yao, C. W. Huang, X. M. Zou, L. Liao, S. S. Chen, Z. Y. Fan, K. Zhang, W. Wu, X. H. Xiao, C. Z. Jiang and W. W. Wu, *Adv. Mater.*, 2016, **28**, 8302-8308.
33. X. X. Li, Z. Q. Fan, P. Z. Liu, M. L. Chen, X. Liu, C. K. Jia, D. M. Sun, X. W. Jiang, Z. Han, V. Bouchiat, J. J. Guo, J. H. Chen and Z. D. Zhang, *Nat. Commun.*, 2017, **8**, 970.
34. X. Cui, E. M. Shih, L. A. Jauregui, S. H. Chae, Y. D. Kim, B. C. Li, D. Seo, K. Pistunova, J. Yin, J. H. Park, H. J. Choi, Y. H. Lee, K. Watanabe, T. Taniguchi, P. Kim, C. R. Dean and J. C. Hone, *Nano Lett.*, 2017, **17**, 4781-4786.
35. A. Avsar, J. Y. Tan, X. Luo, K. H. Khoo, Y. T. Yeo, K. Watanabe, T. Taniguchi, S. Y. Quek and B. Ozyilmaz, *Nano Lett.*, 2017, **17**, 5361-5367.
36. J. Yoon, H. Sung, G. Lee, W. Cho, N. Ahn, H. S. Jung and M. Choi, *Energ. & Environ. Sci.*, 2017, **10**, 337-345.
37. L. Liu, J. W. Lang, P. Zhang, B. Hu and X. B. Yan, *ACS Appl. Mater. & Inter.*, 2016, **8**, 9335-9344.
38. Y. Liu, H. Wu, H. C. Cheng, S. Yang, E. B. Zhu, Q. Y. He, M. N. Ding, D. H. Li, J. Guo, N. O. Weiss, Y. Huang and X. F. Duan, *Nano Lett.*, 2015, **15**, 3030-3034.
39. P. You, Z. K. Liu, Q. D. Tai, S. H. Liu and F. Yan, *Adv. Mater.*, 2015, **27**, 3632-3638.
40. D. K. Nandi, S. Sahoo, T. H. Kim, T. Cheon, S. Sinha, R. Rahul, Y. J. Jang, J. S. Bae, J. Heo, J. J. Shim and S. H. Kim, *Electrochem. Commun.*, 2018, **93**, 114-118.
41. H. J. Wang, H. J. Yu, S. L. Yin, Y. Xu, X. N. Li, Y. Yamauchi, H. R. Xue and L. Wang, *J Mater. Chem. A*, 2018, **6**, 12744-12750.
42. A. S. Aji, P. Solis-Fernandez, H. G. Ji, K. Fukuda and H. Ago, *Adv. Funct. Mater.*, 2017, **27**,

1703448.

43. P. E. Blochl, *Phys. Rev. B*, 1994, **50**, 17953-17979.
44. G. Kresse and J. Furthmuller, *Comp. Mater. Sci.*, 1996, **6**, 15-50.
45. G. Kresse and D. Joubert, *Phys. Rev. B*, 1999, **59**, 1758-1775.
46. J. P. Perdew, K. Burke and M. Ernzerhof, *Phys. Rev. Lett.*, 1996, **77**, 3865-3868.
47. S. Grimme, J. Antony, S. Ehrlich and H. Krieg, *J Chem.l Phys.*, 2010, **132**, 154104.
48. Y. Shao, S. R. Song, X. Wu, J. Qi, H. L. Lu, C. Liu, S. Y. Zhu, Z. L. Liu, J. O. Wang, D. X. Shi, S. X. Du, Y. L. Wang and H. J. Gao, *Appl. Phys. Lett.*, 2017, **111**, 113107.
49. Y. S. Dedkov, M. Fonin, U. Rudiger and C. Laubschat, *Phys. Rev. Lett.*, 2008, **100**, 107602.
50. S. I. Allec and B. M. Wong, *Journal of Physical Chemistry Letters*, 2016, **7**, 4340-4345.
51. W. Hu and J. Yang, *J Mater. Chem. C*, 2017, **5**, 12289-12297.
52. P. Bampoulis, R. van Bremen, Q. R. Yao, B. Poelsema, H. J. W. Zandvliet and K. Sotthewes, *ACS Appl. Mater. & Inter.*, 2017, **9**, 19278-19286.

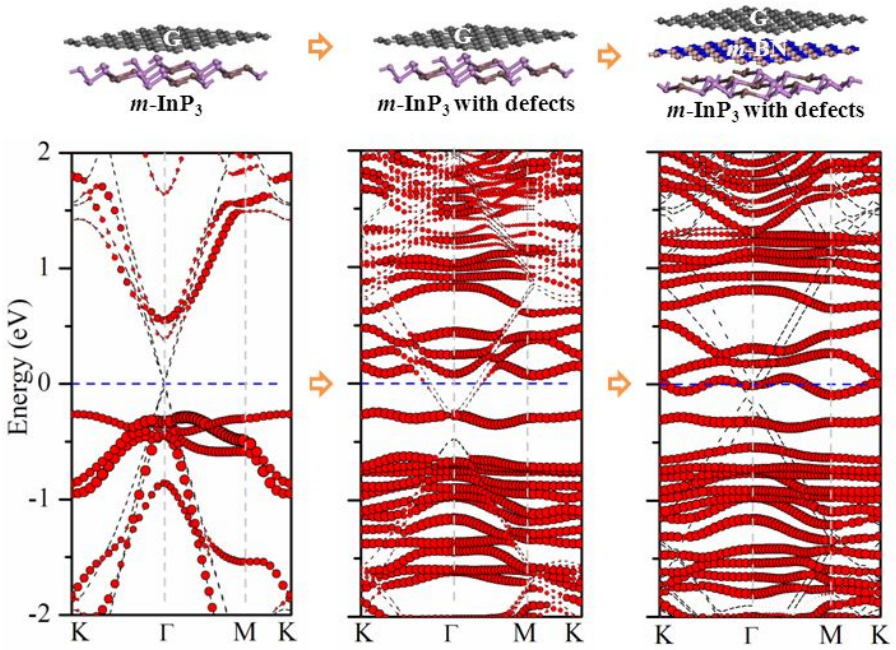

Ohmic contact in m-InP_3 and G or Ni interface is achieved by introducing intrinsic defects and inserting a buffer layer.